Dynamics and Statistics of the Climate System, 2018, 1–13
doi:10.1093/climsys/dzy004
Advance Access Publication Date: 20 December 2018
Research Article

Research Article

Bayesian estimation of englacial radar chronology in Central West Antarctica

Gail R Muldoon[a,b,*], Charles S Jackson[a], Duncan A Young[a] and Donald D Blankenship[a]

[a]University of Texas University of Texas Institute for Geophysics, Jackson School of Geosciences, University of Texas at Austin, Austin, TX, USA and [b]Department of Geological Sciences, Jackson School of Geosciences, University of Texas at Austin, Austin, TX, USA.

*Correspondence Gail R Muldoon, University of Texas University of Texas Institute for Geophysics, Jackson School of Geosciences, University of Texas at Austin, J.J. Pickle Research Campus, Building 196, 10100 Burnet Rd (R2200), Austin, TX 78758, USA; E-mail: gail.muldoon@utexas.edu

Received 19 February 2018; Accepted 5 September 2018

Abstract

Englacial radar reflectors in the central West Antarctic Ice Sheet contain information about past dynamics and ice properties. Due to significant data coverage in this area, these isochronous reflectors can be traced over large portions of the ice sheet, but assigning ages to the reflectors for the purpose of studying dynamics requires incorporation of chronologic data from ice cores. To date reflectors in the Marie Byrd Land region, we consider the Byrd ice core, strategically located between the catchments of Thwaites Glacier and the Siple Coast ice streams. We determine ages with uncertainty for four englacial radar reflectors spanning the ice thickness using Bayesian approaches to combine radar observations, an existing Byrd ice core chronology, and a simplified ice flow model. This method returns the marginal probability distribution of depth and age for each of the observed radar reflectors. The results also include inferences of accumulation rate at the Byrd ice core site during the last 30 ka that show a minimum accumulation rate during the Last Glacial Maximum at half the modern rate. The deepest continuous radar reflector is 25.67 ± 1.45 ka, <30% of the estimated age of the oldest ice at the Byrd ice core site despite being located at 70% of the ice depth, limiting the age of radar-interpretable ice in this region. The inferred reflector age profiles at the Byrd ice core site derived here compare favourably with the more recent WAIS Divide ice core record. However, uncertainty in reflector depth due to radar range precision contributes considerably to uncertainty in reflector age in a way that is not readily reducible using currently available ice-penetrating radar systems.

Key words: airborne radio-echo sounding, Bayesian estimation, ice chronology/dating, ice flow modelling, ice sheet accumulation rate.

1. Introduction

Isochronous, englacial radar reflectors observed by ice-penetrating radar record the depth and extent of isosurfaces with shared physical properties (Siegert *et al.*, 1998; Dowdeswell and Evans, 2004). These reflectors can map the age structure of an ice sheet, with the thickness of layers bounded by reflectors revealing information about ice flow dynamics and variable ice properties. Such observations have been used in Greenland and Antarctica to infer the ice flow history of the ice sheets in response to changing climate regimes in the past (MacGregor *et al.*, 2015). To provide such historical climatic context, reflectors are assigned ages by correlation to a known chronology, such as at an ice core site (Cavitte *et al.*, 2016). Dating englacial reflectors enables information from the entire ice volume, not only surface observations, to constrain ice sheet dynamics. However, combining information from ice cores and radar observations is intrinsically complicated by the fact that ice core chronologies assign discrete ages to samples of ice, while radar reflectors track packets of ice with finite thickness that span a range of ages, particularly at depth where age is more sensitive to depth due to shear thinning of the ice.

To understand how well radar reflectors can be dated, we use Bayesian methods to synthesize information from ice cores, radar sampling, ice flow modelling, and our knowledge of the leading sources of uncertainty within the radar and ice core data sources. We apply our approach to the central West Antarctic Ice Sheet (WAIS), an area containing the potential for unforced retreat where ice dynamics are of particular interest for projections of future sea-level rise. In addition to being of scientific importance, the central WAIS is an area with concentrated radar surveys and two deep ice cores, the Byrd ice core (Gow *et al.*, 1968). In particular, the proximity of the Byrd ice core (80.0167°S, 119.5167°W) to fast-changing ice of both the Siple and Amundsen Sea coasts in West Antarctica makes it a potentially important source of information about the response of the WAIS to climate change.

The Byrd ice core is co-located with several extensive radar surveys (Fig. 1) and contains an ice record that extends back to >90 ka (Blunier and Brook, 2001), nearly back to the Last Interglacial. Rather than use existing chronologies for the age–depth relationship at the Byrd ice core, which do not sufficiently characterize its uncertainty, we generate our own chronologies using Bayesian strategies to synthesize an ice flow model with age–depth data obtained from volcanics sampled from the Byrd ice core (Gow *et al.*, 1968; Gow, 1970; Hammer *et al.*, 1997). This method allows us to simulate the co-dependence in dating errors within and between different radar reflectors.

The four reflectors in this study were chosen as a representative sample of the ice column and for their signal-to-noise ratio (SNR) and continuity. It is possible to use this method to date additional englacial reflectors observed using radar in this area, but the usefulness of such ages extend only as far as the isochronous reflectors can be horizontally traced. While this method is less helpful for dating discontinuous reflectors, it could inform relative ages for sections of discontinuous reflectors adjacent to dated reflectors in the ice column (e.g. MacGregor *et al.*, 2015).

We consider two quantities of interest in this problem: radar-inferred depths from observed two-way travel time (TWTT) and dated volcanics from the Byrd ice core. The primary sources of uncertainty in radar depths include the speed of electromagnetic radiation in ice, the density and thickness of the firn layer, and radar range precision. The error on range precision is determined independently for each reflector and the ice surface, while errors in velocity and firn are systematic (common) across all reflectors of interest in the ice column which are deeper than the firn layer. This is because we assume constant velocity in ice and all reflectors below the firn will be equally affected by any depth error accumulated as the signal passes through the firn layer. To estimate the ages of reflectors, we make use of dates determined for volcanic markers in the ice column (Hammer *et al.*, 1997). In the absence of published uncertainty in the volcanic record, we use a Bayesian strategy to compute the unknown reflector age uncertainty. An ice flow model is used to smoothly transfer information from the volcanics to the estimated depth of our reflectors of interest. To do so, it is necessary to infer flow physics parameters and accumulation rate history. Estimated ice flow and accumulation rate parameters are dependent on one another and on depth and are applied to the full ice column. A Bayesian framework allows us to describe all components of the problem within a single calculation, but requires stochastic sampling to estimate the marginal probability of reflector depth (and therefore age) as a function of observed TWTT and volcanics.

Section 2 discusses the formulation of the Bayesian problem and methods for finding solutions of the age and depth of observed englacial radar reflectors. Section 3 shows results for the probability distributions of reflector age and depth as well as a comparison to the WAIS Divide ice core chronology as an independent check on our results. We also calculate an error budget to determine the dominant contributions to age–depth uncertainty, discussed in Section 4.

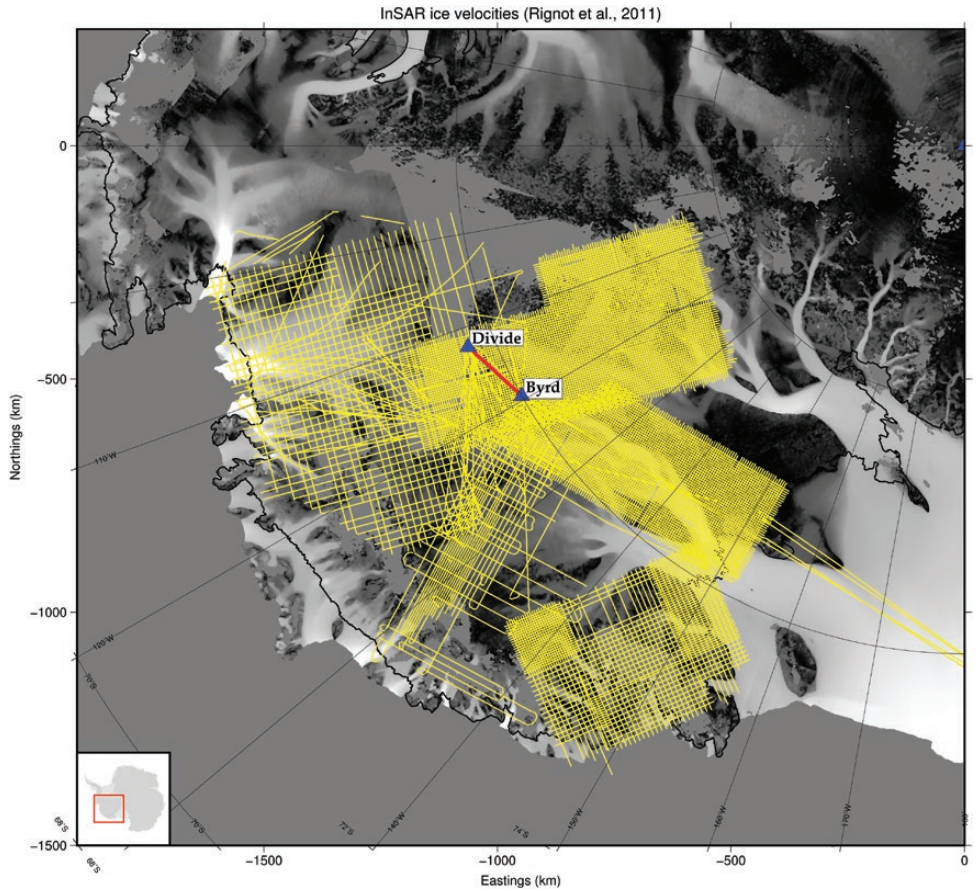

Figure 1. Map of central West Antarctic with available airborne geophysical radar surveys (yellow lines) and WAIS Divide and Byrd ice core locations (blue triangles) overlain. Grey shading is surface velocity (Rignot et al., 2011). The red line denotes the flight line along which the reflectors in this study were observed.

2. Posterior distribution of englacial reflector age–depth

In order to assign ages to observed radar reflectors, we are interested in combining information from radar, ice flow physics and dates from ice core volcanics at the Byrd ice core site. To do so, we take advantage of the versatility of a Bayesian approach to assemble the desired solution from a set of inter-related components. Our method preserves the chronologic superposition of the ice column and correlation of errors with depth, estimates the probability of ice flow parameter values and estimates a marginal probability of the age–depth profile.

The Bayesian formulation of the posterior probability distribution of radar reflector age is as follows:

$$\begin{aligned}&\mathrm{PPD}(A_r) = \mathrm{PPD}(D_r, \vec{f}, v_{ice}, S|\mathrm{TWTT}_r, A_{IC}, D_{IC}) \propto \\ &p(\mathrm{TWTT}_r|D_r, v_{ice}) \cdot p(A_{IC}, D_{IC}|\vec{f}, S) \\ &\cdot p(D_r) \cdot p(\vec{f}) \cdot p(S) \cdot p(v_{ice})\end{aligned} \tag{1}$$

Computing the posterior probability distribution of reflector ages, $\mathrm{PPD}(A_r)$ in Equation 1, requires jointly estimating the depths of the englacial reflectors of interest (D_r), ice flow model parameters and accumulation rate history ($\vec{f}$), radar velocity in ice (v_{ice}) and precision of the Byrd ice core chronology (S). We estimate these values given information about observed radar reflector two-way travel time (TWTT_r) and the ages and depths of volcanics (A_{IC}, D_{IC}) interpreted from the Byrd ice core record (Hammer *et al.*, 1997).

We use priors, the rightmost four terms in Equation 1, to put physical bounds on sources of uncertainty as described in the following sections. Priors on D_r also preserve stratigraphic dependence of radar reflectors, requiring deeper reflectors be older than shallower reflectors. Likelihood functions, the first two terms on the right-hand side of Equation 1, evaluate if ice flow and radar model estimates are consistent with observations. The age likelihood (second term on right-hand side of Equation 1) tests whether sampled ice flow parameters and accumulation rate history ($\vec{f}$) generate age–depth profiles consistent with the volcanic ages and depths (A_{IC}, D_{IC}). The scatter between modelled and observed ages determines precision (S) and whether estimates of D_r and v_{ice} are rejected or accepted relative to previously accepted solutions. The TWTT likelihood (first term on right-hand side of Equation 1) tests agreement between observed two-way travel time ($TWTT_r$) and modelled TWTT using reflector depths (D_r) and v_{ice}. Both likelihood tests are used to accept or reject various 'steps' through this solution space, resulting in an ensemble of accepted solutions. The elements of Equation 1 are discussed more thoroughly in subsequent sections.

2.1. Ice flow model at the Byrd ice core

Due to the inherent stratigraphic dependence of age in the ice column and the nonlinear effect of ice deformation on layer depths, we use a flow model to simulate the age–depth relationship. We use a simple, 1D model of ice flow (Equation 2), which derives ice age from accumulation and strain rate, assuming constant horizontal strain rate in the upper part of the ice sheet and a shear layer of thickness h at the base of the ice sheet (Schwander *et al.*, 2001). In the shear layer, the strain rate is assumed to decrease linearly and the bottom of the ice is assumed to slide with velocity $q \cdot v_0$, where v_0 is the horizontal velocity at the surface. The age of ice as a function of elevation from the bedrock interface is therefore:

$$A(z) = \int_z^H \frac{dz}{\varepsilon_z \cdot \dot{a}(z)} \tag{2}$$

where strain is described by

$$\varepsilon_z = \begin{cases} 1 - k(H - z), & h \le z \le H \quad \text{(upper)} \\ kz\left(q + \frac{1-q}{2h} z\right), & 0 \le z < h \quad \text{(lower)} \end{cases},$$

and k is a constant such that $k = \frac{2}{2H - h(1-q)}$. H is ice thickness, which has been observed to be 2164 m at the Byrd ice core site (Gow *et al.*, 1968) and z is the height above the bed. We invert for the remaining parameters: h, the depth to the Dansgaard–Johnsen shear (Dansgaard and Johnsen, 1969); $\dot{a}$, the time-dependent accumulation rate; and q, the ratio of horizontal velocity at the surface to that at the bed of the ice sheet.

The ice flow model accounts for two primary factors in the age–depth profile: burial as a function of accumulation rate, $\dot{a}$, and thinning as a function of strain, ε_z. In the simplest realization, ice deposited at a given time at the ice sheet surface will be found at a depth corresponding to the amount of subsequent accumulation. However, due to strain thinning at depth, ice of a given age will be less deep than would be expected if accumulation alone is considered.

The priors used for the ice flow parameters are defined by:

$$p(\vec{f}) = \begin{cases} p(h) \sim U\,[0, 0.5] \\ p(q) \sim U\,[0, 1] \\ p(\dot{a}_{i,i=1\ldots10}) \sim U\,[0.05, 0.25]\, m/a \end{cases} \tag{3}$$

The prior distributions of flow parameters and accumulation rate history, together denoted as $p(\vec{f})$, assume the shear layer is in the bottom half of the ice sheet depth (Cuffey and Paterson, 2010) and that ice at the bed of the ice sheet is moving no faster than the surface, which would allow for cases of both plug and creep flow. Accumulation rate as a function of depth, $\dot{a}$, is estimated for 10 distinct depth bins spanning the ice thickness at 200-m intervals. The use of 10 discrete bins allows for a straightforward way to capture the variability of accumulation rate over time. We found that increasing the number of accumulation rate bins did not affect the result.

2.2. Radar depth and error model

Radar pulses transmitted into the ice sheet reflect off surfaces of dielectric contrast in the ice that are the result of variations in ice fabric, composition, temperature and rheology of ice (Fujita *et al.*, 2000). The reflected signal is received by the radar system and recorded as TWTT from transmission to receipt. The reflector data in this analysis (Fig. 2) were collected by the University of Texas Institute for Geophysics, including GIMBLE (Young *et al.*, 2017), AGASEA (Holt *et al.*, 2006), CASERTZ (Morse *et al.*, 2002) and SOAR/WMB (Luyendyk *et al.*, 2003) (Fig. 1). Data used to trace reflectors between Byrd ice core and WAIS Divide ice core were collected from a DC-3 or Twin Otter airborne platform and used the HiCaRS2 coherent radar system with 60 MHz centre frequency and 15 MHz bandwidth (Young *et al.*, 2016).

In this study, we consider TWTT of four reflectors spanning the ice thickness in the region of central West Antarctica (Fig. 2). These reflectors have been tracked using Halliburton's Landmark seismic interpretation software and can be tied to both the Byrd and WAIS Divide ice cores for dating using observations from the HiCARS system (Fig. 1).

To estimate reflector depths from TWTT ($\mathrm{TWTT}_{m,r}(D_r)$), we use a simple relation between the different velocities of the radar signal in air and ice and incorporate several known sources of uncertainty, including (i) variations in the radar velocity in ice due to ice temperature and fabric (v_{ice}), (ii) vertical precision limitations of radar range detection (σ_{prec}) and (iii) uncertainty in the firn correction ($\varepsilon_{\mathrm{firn}}$) due to measurement errors in the ice density profile:

$$\mathrm{TWTT}_{\mathrm{m},r}(D_r) + \sigma_{\mathrm{prec},r} = 2\frac{D_r - (d_{\mathrm{firn}} + \varepsilon_{\mathrm{firn}})}{v_{ice}} + (\mathrm{TWTT}_{\mathrm{surf}} + \varepsilon_{\mathrm{prec,surf}}) \tag{4}$$

The complexity of local ice properties affecting the velocity at any location and depth makes it difficult to know the true velocity. Empirical evidence suggests a range of expected velocities, and we conservatively assume they are uniformly distributed such that $p(v_{\mathrm{ice}}) \sim U[168, 169.5]$ m/μs (Fujita *et al.*, 2000). In lieu of detailed observations of ice properties with depth, we assume the value of v_{ice} is a constant throughout the ice column and apply it systematically to all reflector depths.

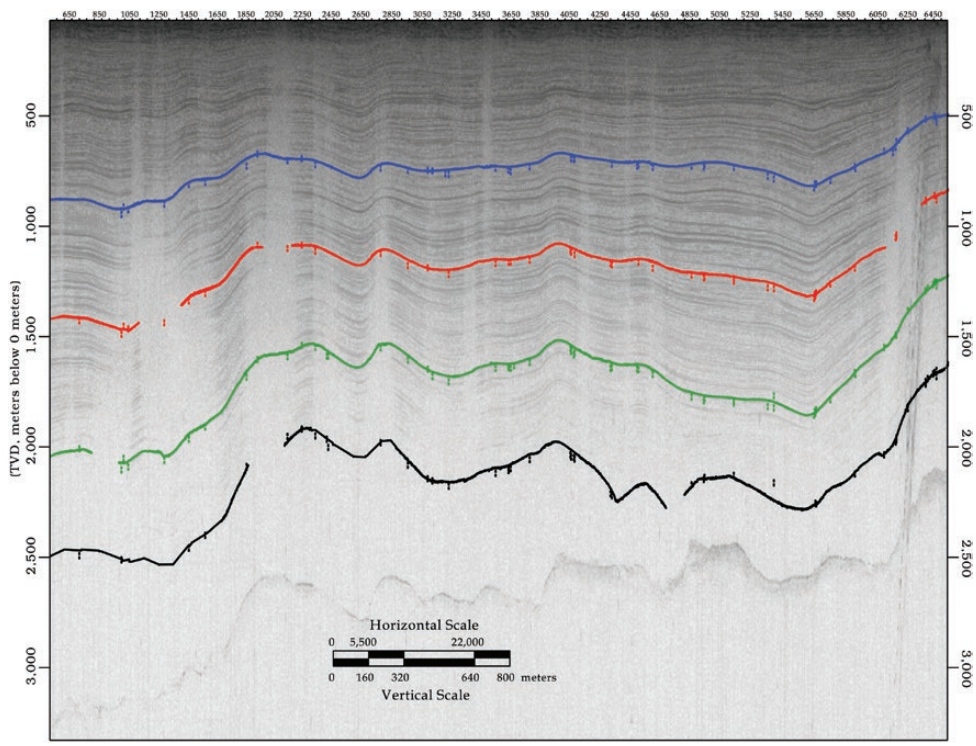

Figure 2. Radargram showing reflectors of interest near the Byrd ice core along flight line ICP6/MKB2I/F14T01a observed using the HiCARS2 radar system. Short vertical hatches along tracked reflectors show intersections with crosslines.

The radar pulse width determines vertical precision, $\sigma_{\text{prec},r}$ (Millar, 1982). We assume a finite pulse width, meaning an infinitesimally thin layer of ice will appear in the survey to have a finite width. This can lead to errors in tracing isochronous reflectors, as the reflected energy from a finite depth will include ice with a range of ages. To account for this, we include uncertainty due to range precision, according to the SNR of each reflector's radar amplitude as in Cavitte *et al.* (2016):

$$\sigma_{\text{prec},r} = \frac{\Delta r}{\sqrt{\text{SNR}_r}} \tag{5}$$

The range resolution, Δr, is 8.4 m for all reflectors in the HiCARS2 system (Young *et al.*, 2011). Values of the SNR for each reflector are shown in Table 1.

Finally, a firn layer with variable density (Gow, 1970) exists in the upper part of the ice sheet. The velocity of the radar is faster in firn than in solid ice. To correct for the underestimation of ice depth if the firn layer is not considered, we estimate the firn correction (d_{firn}), the difference between the ice thickness with and without the firn layer present. Errors in density, $\rho(z)$, are used to estimate the error in d_{firn}, $\varepsilon_{\text{firn}}$. These errors are known for the WAIS Divide measurements, but not for the Byrd ice core profile. In lieu of density measurement errors at the Byrd site, we assume the errors to be consistent with those observed at the WAIS Divide ice core. These errors are assumed Gaussian, randomly sampled, and the firn correction is computed using the Dowdeswell and Evans' (2004) relation:

$$d_{\text{firn}} = \frac{K}{n'_i} \int (\rho_i - \rho(z))dz \tag{6}$$

where K is 0.85 m^3/Mg (Robin *et al.*, 1969), n'_i is the refractive index of ice (n'_i = 1.78), ρ_i is the density of ice (ρ_i = 0.917 Mg/m) and $\rho(z)$ is the density of ice at depth z with units Mg/m.

The TWTT from the observing aircraft to the surface of the ice sheet is known from interpretation of the surface reflector, $\text{TWTT}_{\text{surf}}$. The computed depth of each reflector is relative to this surface reflector. Just as each reflector may have TWTT precision errors independent of the others, errors in the distance between the surface and the acquisition aircraft are common to all observed reflectors in the ice column. Therefore, a randomly sampled precision error, $\varepsilon_{\text{prec,surf}}$, is applied systematically to all reflectors.

2.3. Metropolis algorithm

At each iteration, a hybrid of Hastings and Gibbs sampling (Hastings, 1970; Gelfand *et al.*, 1992) is used to select values for parameters of interest (those with priors in Equation 1). The algorithm accepts or rejects proposed sets of parameter values by comparison between the proposed and previously accepted values, as measured by the likelihood. A high likelihood value represents good agreement between model and observations. According to the Hastings algorithm, if the likelihood associated with proposed parameters is higher than that of the previous accepted iteration, the proposed parameter values are accepted. Alternatively, lower likelihood values may be accepted with a probability determined by the change in likelihood.

There are two likelihood functions describing the model-data misfit in reflector depth and age, respectively:

Table 1. Depth and age mean and standard deviation for four radar reflectors near Byrd Station, West Antarctica used in this study

Reflector	TWTT (μs)	Depth (m)		Age (a)		SNR (dB)
		μ	α	μ	α	
1	8.44	510.1	13.1	4711	246	10.41
2	12.54	854.6	18.0	8653	318	8.13
3	17.55	1277.9	10.8	17177	413	11.63
4	22.42	1460.0	5.2	24928	286	21.22

The radar-observed TWTT to each reflector and its associated SNR used to compute TWTT uncertainty is also shown. SNR, signal-to-noise ratio; TWTT, two-way travel time.

$$p(\mathrm{TWTT}_r|D_r,\ d_{\mathrm{firn}}, v_{\mathrm{ice}}) \propto \exp\left[\frac{-\sum_{r=4}[\mathrm{TWTT}_r - \mathrm{TWTT}_{m,r}(D_r)]^2}{2\sigma^2_{\mathrm{TWTT}}}\right] \tag{7}$$

$$p(A_{\mathrm{IC}}|D_{\mathrm{IC}}, \vec{f}, S) \propto \exp\left[\frac{-S\sum_{j=61}[A_{\mathrm{IC},j} - A_{m,j}(\vec{f}, D_{\mathrm{IC}})]^2}{2\sigma^2_{\mathrm{A}}} + R^6\right] \tag{8}$$

Both likelihood functions must lead to acceptance in order for the proposed parameters to be accepted.

In the depth likelihood function, $\mathrm{TWTT}_{m,r}(D_r)$ is based on the relationship between estimates of D_r and TWTT as in Equation 4. TWTT_r is observed by ice-penetrating radar for each reflector, r. Uncertainty in TWTT, σ_{TWTT}, is taken to be the same as the radar range precision error, which is a function of the signal-to-noise of each reflector amplitude and the bandwidth of the HiCARS radar system as described previously.

In the age likelihood function, the modelled age, A_{m}, is a function of ice flow model parameters and accumulation rate history, $\vec{f}$. A regularization term, R^6, is used to penalize large variability in the accumulation rates input to the ice flow model. R is a constant for each proposal equal to the ratio of the variance of the smoothed to unsmoothed proposed accumulation function. A_{m} comes from solutions to the forward ice flow model. We use $j = 61$ volcanic events from Hammer *et al.* (1997) as the observational target, A_{IC}, which do not include uncertainty information. These data represent dated volcanic deposits observed in the Byrd ice core and extend to ~50 ka, though there is a lack of data in the brittle zone of the ice core between 300 and 900 m depth where the electrical conductivity cannot be measured (Hammer *et al.*, 1997). Age uncertainty, σ_{A}, is nominally taken to be 1% of reflector age, a presumed underestimation of the true uncertainty. To determine additional uncertainty in volcanic age, we include a precision parameter, S, and use it to infer uncertainty in the volcanic record from scatter between our model and the observed data. In Bayesian nomenclature, S is a 'nuisance' parameter that accounts for uncertainty in σ_{A} by using the sum of squared errors, E_{m}, as a measure of scatter between modelled age, A_{m}, and observed volcanic age, A_{IC}.

The posterior probability distribution of S is:

$$\mathrm{PPD}(S) = Ga\left(\frac{k_e}{2} + \alpha, E_m + \beta\right) \tag{9}$$

where

$$E_m = \frac{\sum_j [A_{IC,j} - A_{m,j}(\vec{f}, D_{IC})]^2}{2\sigma^2_A} \tag{10}$$

Parameters α and β are assumed to be 1 as in the case for a non-informative gamma prior, $p(S) \sim Ga(\alpha, \beta)$. Unlike other parameters in our problem, values of S are selected through Gibbs sampling (Gelfand *et al.*, 1992), effectively estimating reflector age uncertainty given the choice of ice flow model parameters and accumulation rate history for each iteration.

3. Dated englacial reflectors at the Byrd ice core

3.1. Reflector age and parameter estimates

The marginal probability distributions (1D projections of the joint probability) of age and depth derived for englacial radar reflectors observed at the Byrd ice core site are shown in Figure 3 and Table 1. The age of the observed reflectors increases with depth, as expected due to stratigraphic burial of ice as it is deposited at the ice sheet surface. However, uncertainty in depth (and therefore age) does not increase monotonically with depth because of its dependence on reflector SNR, as discussed in the next section.

We estimate the oldest continuous radar reflector in central West Antarctica to be 24.9 ± 0.3 ka despite being observed at only 68% of the ice column depth (1466 ± 5 m). While this constrains the age of ice near the bed of the ice sheet, it also limits the ability to use radar observations in this area to directly study ice sheet dynamics before the

Last Glacial Maximum. Reflector 3, the second deepest reflector, is dated to 17.2 ± 0.4 ka, which is consistent with the estimated age of the 'Old Faithful' reflector, believed to be a relict from a series of volcanic eruptions. Reflectors 1 and 2 sample the ice column during the last 10 ka.

As has been established in previous work (Siegert *et al.*, 1998; Dowdeswell and Evans, 2004), we assume radar reflectors are isochronous such that their age is the same whether observed at the Byrd ice core or the WAIS Divide ice core. To compare between the two ice cores, we use Halliburton's Landmark seismic interpretation software to track radar reflectors through central WAIS via an existing radar survey flight line (Fig. 1). The age–depth profiles at the Byrd ice core site (this study) and the WAIS Divide ice core effort (Buizert *et al.*, 2015) are shown in Figure 4. Mean

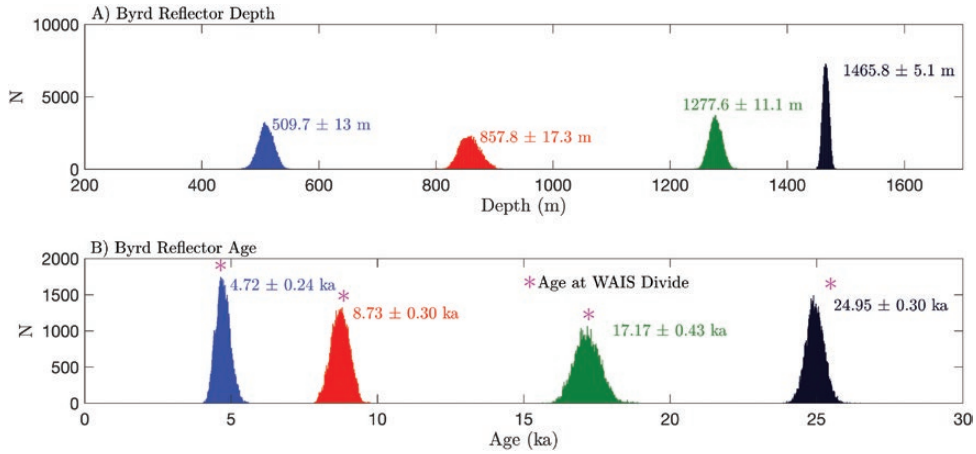

Figure 3. Posterior probability distributions of depth (top) and age (bottom) of four radar reflectors at the Byrd ice core. The width of the age and depth histograms for the Byrd ice core chronology represent uncertainty estimated by the methods used here.

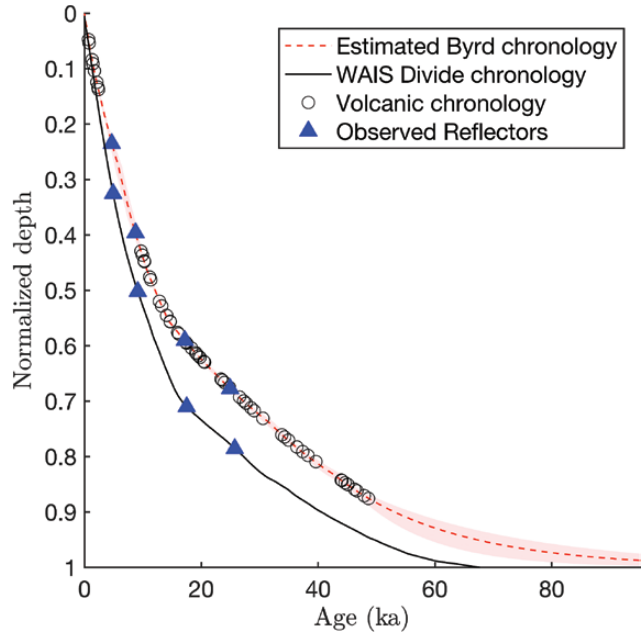

Figure 4. Modelled age–depth relationship with uncertainty compared with measured volcanic chronology from Hammer et al. (1997) (open circles). The WAIS Divide ice core chronology (Buizert et al., 2015) as a black line. Blue triangles show the age–depth of four radar reflectors at each of the Byrd and WAIS Divide ice cores; these reflectors are assumed isochronous and so expected to be the same age at either ice core.

estimated age for each reflector at the Byrd ice core site compares favourably to that computed at the WAIS Divide ice core site (Fig. 4).

In addition to computing the age and depth of radar reflectors, our method includes inversion for a number of parameters related to ice flow and paleo accumulation rates (Table 2). Posterior probability distributions for these parameters are shown in Figure 6. Estimates of accumulation rate are uncertain, particularly in the brittle zone of the Byrd ice core (300–900 m) where volcanic data are not available and corresponding posterior distributions look most non-Gaussian. The widest, most uncertain accumulation rate posterior distribution represents depths below the deepest volcanic records (~1850 m), where there is limited constraint on the estimate. Even with these limitations, the general pattern of estimated accumulation rate reflects an expected pattern of lower accumulation rate during the Last Glacial Maximum (~1500 m), where we infer accumulation rates about half that of the modern (Fig. 5).

Posterior probability distributions for other ice flow parameters estimated by the model are also shown in Figure 6. The ratio of surface to bed velocity, q, is inferred to be 0.9 ± 0.08 (where a ratio of 1 would indicate plug flow), indicating near plug flow at the Byrd ice core, which is consistent with the presence of liquid water at the ice sheet

Table 2. Mean and standard deviation of parameter values estimated in this study and used to estimate reflector age and depth

Parameter	Median ± 1σ	Parameter	Median ± 1σ
$\dot{a}$ (d < 200 m)	14.8 ± 0.2 cm	q	0.9 ± 0.08
$\dot{a}$ (200 m ≥ d < 400 m)	11.4 ± 0.6 cm	h	0.45 ± 0.03
$\dot{a}$ (400 m ≥ d < 600 m)	11.1 ± 1.4 cm	v_{ice}	1.684 ± m/s
$\dot{a}$ (600 m ≥ d < 800 m)	14.2 ± 1.2 cm	S[a]	0.154; (0.06, 0.32)
$\dot{a}$ (800 m ≥ d < 1000 m)	13.0 ± 1.8 cm		
$\dot{a}$ (1000 m ≥ d < 1200 m)	11.2 ± 0.7 cm		
$\dot{a}$ (1200 m ≥ d < 1400 m)	6.8 ± 0.3 cm		
$\dot{a}$ (1400 m ≥ d < 1600 m)	7.2 ± 0.5 cm		
$\dot{a}$ (1600 m ≥ d < 1800 m)	9.2 ± 1.0 cm		
$\dot{a}$ (1800 m ≥ d)	11.6 ± 2.5 cm		

[a]Values provided for S are the median and 95% confidence interval.

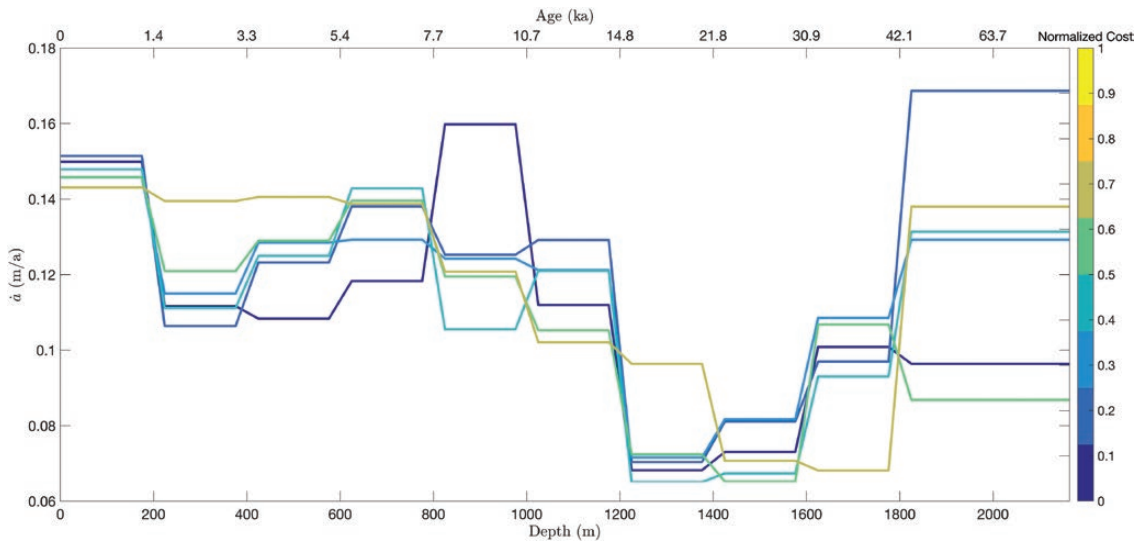

Figure 5. Accumulation rate as a function of ice depth coloured by cost value which reflects each solution's fit to data. (Accumulation rate functions associated with lower cost are expected to be better solutions.) Accumulation rate is estimated in 10 depth bins at ~200-m-depth intervals. Transitions between these intervals have been smoothed in this figure for ease of viewing.

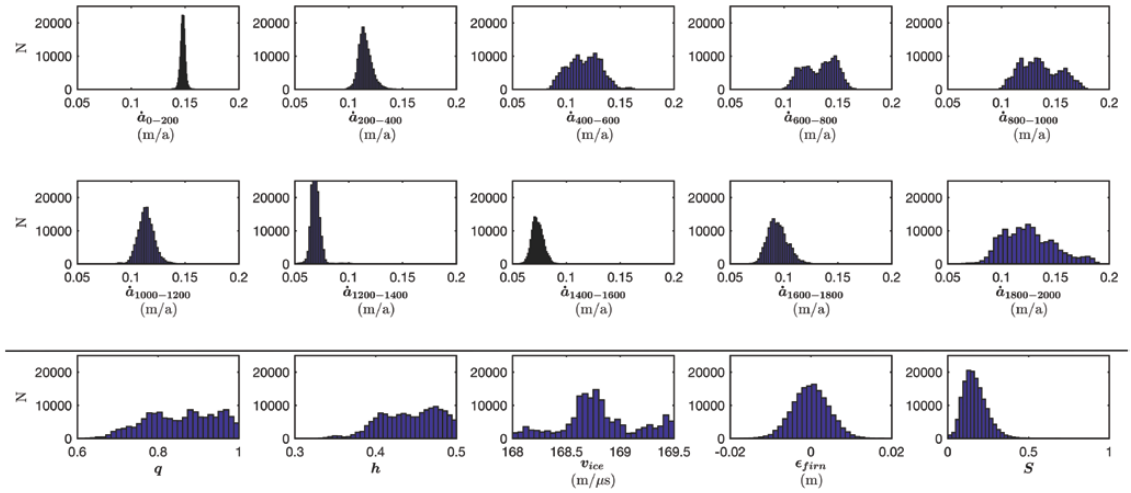

Figure 6. Posterior probability distributions of inverted parameters, including accumulation rate, q, h, v_{ice}, ε_{firn}, and S. Accumulation rate parameter values are assigned to 200-m-depth intervals indicated by the subscript. While a few parameter distributions appear non-Gaussian, parameter values are well sampled and generally single peaked. The precision parameter, S, has an expected gamma distribution, and ε_{firn} is normally distributed, as expected.

base found during drilling. The transition depth, h, is not well constrained by our estimates, probably because of the near-plug-flow conditions inferred by our model.

We estimate the mean radar velocity through ice, v_{ice}, to be 168.4 m/μs, which is in the middle range suggested by empirical estimates, but our posterior probability distribution shows secondary peaks. Estimates of the precision parameter S imply 2.5% uncertainty in reflector age with a 95% confidence interval of (1.8%, 4.11%) (from $S \sim \frac{1}{\sigma^2}$), consistent with values that have been reported in ice core chronologies.

3.2. Error budget

To evaluate how much errors in each parameter contribute to uncertainties in age and depth of radar reflectors, we consider how uncertainty in reflector age and depth change when each parameter is assumed to be known with no error. To do so, we hold each model parameter fixed at its optimal value (Fig. 3). If there is no change in the distribution of reflector age and depth, error in that model parameter has no influence on the result.

We find errors in depth contribute 25%, 37%, 77% and 43% to uncertainty in depth to reflectors 1, 2, 3 and 4, respectively. This suggests that deeper in the ice column an increasing portion of uncertainty in age is from errors in reflector depth. However, high reflector SNR (and therefore radar range precision) can mitigate this effect. As seen in Figure 3, the deepest observed reflector, which may be expected to have the largest depth uncertainty, instead has relatively high SNR and therefore low uncertainty.

Uncertainty in age is also sensitive to the accumulation rate profile, which accounts for up to 40% of the age uncertainty of each reflector. Accumulation rates in localized portions of the ice column do not individually influence the age uncertainty as much as the full accumulation rate profile, but rates in the upper part of the ice column have more impact due to their influence on the age of ice below. Other individual ice flow parameters play a far smaller role in the error budget.

4. Discussion

For this study, we use a simple Dansgaard–Johnsen-type ice flow model (Schwander *et al.*, 2001). We do not include a separate term for basal melting, which is probably occurring or has occurred at this site as liquid water was observed at the bed during drilling (Gow *et al.*, 1968). The inclusion of a melt condition is expected to increase accumulation rate estimates to account for ice loss at the bedrock interface. We exclude basal melting because we lack estimates of basal melt rate over time. However, this method could be adapted to incorporate a more sophisticated flow model with additional parameters such as a non-zero melt rate.

To estimate the ice flow and accumulation rate parameters in our model, we must assume the effective number of degrees of freedom, k_e, because it is not known. The number of degrees of freedom helps determine the significance of errors between our model and the volcanic chronology. Because we use these errors as a measure of uncertainty through paramater S, k_e has a direct role in determining the uncertainty in age estimates. Estimates of k_e using our ice flow model to represent the effect of uncertainites in ice flow parameters and accumulation rates on age estimates varied depending on assumptions about these model parameters. Given this variation and the potentially circular logic in this method, we instead choose $k_e = \frac{j}{2} = 30.5$, which assumes there are strong correlations among age solutions. This is reasonable because we expect errors in age and depth are related within the ice column.

As shown in Figure 7, this choice does not affect mean estimates of reflector age and depth, but it does have some affect on the uncertainty associated with them.

Uncertainties in our estimates of radar reflector depth are significant compared with those derived from the age determination alone. These relatively large uncertainties from the radar can be attributed to radar range precision in the determination of reflector depths. This precision is a function of the SNR of the radar reflection and bandwidth of the radar system used to obtain the reflections (Cavitte *et al.*, 2016). Increasing SNR would improve range precision and reduce uncertainty; however, our method already selects for high SNR in analysing only the brightest reflectors in the ice column. As a result, we expect the data do not support improving precision in this way. Increasing bandwidth (15 MHz for the HiCARS radar system) would also improve the radar range precision; however, this is technically challenging for modern airborne radar systems because antenna tuning is difficult for bandwidths greater than 25% of the centre frequency (60 MHz for the HiCARS system). Ground penetrating radar systems can have higher bandwidth, but are more limited in their spatial coverage. Furthermore, while higher resolution can be obtained by increasing bandwidth and centre frequency, penetration through the ice declines and reflections become increasingly discontinuous with increasing bandwidth (Cavitte *et al.*, 2016).

5. Conclusion

We derive ages for isochronous radar reflectors observed near the Byrd ice core which include estimates of uncertainty in ice flow parameters and accumulation rates in the region of Marie Byrd Land, West Antarctica. Such radar

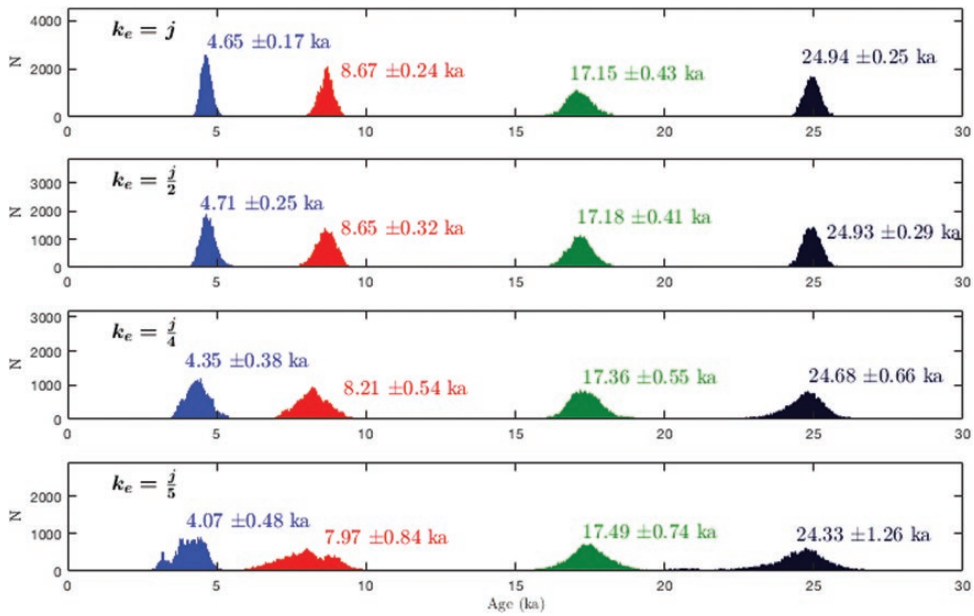

Figure 7. Comparison of reflector age for different degrees of freedom, k_e, relative to the number of volcanic data points, $j = 61$. The choice of k_e has an effect on uncertainty in reflector age estimates, but does not greatly impact mean estimates.

observations may reveal englacial stratigraphy indicative of past ice flow, but require dating to put constraints on interpretations of ice dynamics. The Byrd ice core location connects WAIS Divide to the ice streams of the Siple Coast and the Marie Byrd Land icecap via radar observations, and this work contributes to constraining uncertainty in the chronology of englacial radar reflectors.

Our estimates of the reflector age–depth are consistent with independent comparison to the same reflectors dated using the WAIS Divide ice core chronology (Buizert *et al.*, 2015), although large uncertainties due to radar range precision preclude a strong test of inferences between the two cores. Our results indicate the oldest continuous radar reflector dateable using existing ice cores and radar surveys in central West Antarctica is located at ~70% ice depth at the Byrd ice core site and dates to ~24.9 ± 0.3 ka. The same reflector is observed at ~80% ice depth in the WAIS Divide ice core. While the Byrd ice core has been dated to as old as ~94 ka at its base (Blunier and Brook, 2001), continuous radar reflectors do not extend deep enough in this region to leverage the ice core to date older radar-observed ice in the central WAIS. The range precision of existing ice-penetrating radar systems is the biggest contributor to uncertainty in radar reflector age. This uncertainty is largely irreducible due to practical trade-offs in airborne system design and leads to potentially significant uncertainty in reflector age at depth.

Declaration

Funding: University of Texas Institute for Geophysics; CDI (NSF Grant #OPP-0941678); SPICECAP (NSF Grant #PLR-1443690); GIMBLE (NSF Grant #PLR-1043761); The G. Unger Vetlesen Foundation.
Ethical approval: none.
Conflict of interest: none.

Acknowledgements

The authors thank UTIG radar interpreters including Robert Stephany, Shubhanga Ballal, Arami Rosales, Rebekah Albach and Varun Sudunagunta.

References

Blunier T, Brook EJ. Timing of millennial-scale climate change in Antarctica and Greenland during the last glacial period. *Science* 2001; 291: 109–12.

Buizert C, Cuffey KM, Severinghaus JP et al. The WAIS Divide deep ice core WD2014 chronology–Part 1: methane synchronization (68–31 ka BP) and the gas age–ice age difference. *Clim Past* 2015; 11: 153–73.

Cavitte MG, Blankenship DD, Young DA, et al. Deep radiostratigraphy of the East Antarctic plateau: connecting the Dome C and Vostok ice core sites. *J Glaciol* 2016; 62: 323–34.

Cuffey KM, Paterson WSB. *The Physics of Glaciers*. Cambridge: Academic Press, 2010.

Dansgaard W, Johnsen SJ. A flow model and a time scale for the ice core from Camp Century, Greenland. *J Glaciol* 1969; 8: 215–23.

Dowdeswell JA, Evans S. Investigations of the form and flow of ice sheets and glaciers using radio-echo sounding. *Rep Prog Phys* 2004; 67: 1821.

Fujita S, Matsuoka T, Ishida T, Matsuoka K, Mae S. A summary of the complex dielectric permittivity of ice in the megahertz range and its applications for radar sounding of polar ice sheets. *Phys Ice Core Rec* 2000; 185–212. https://eprints.lib.hokudai.ac.jp/dspace/bitstream/2115/32469/1/P185-212.pdf

Gelfand AE, Smith AF, Lee T-M. Bayesian analysis of constrained parameter and truncated data problems using Gibbs sampling. *J Am Stat Assoc* 1992; 87: 523–32.

Gow AJ. *Preliminary Results of Studies of Ice Cores from the 2164 m Deep Drill Hole*, Vol. 86. Byrd Station, Antarctica: IAHS Publication, 1970, pp. 78–90.

Gow AJ, Ueda HT, Garfield DE. Antarctic ice sheet: preliminary results of first core hole to bedrock. *Science* 1968; 161: 1011–3.

Hammer C, Clausen H, Langway C. 50,000 years of recorded global volcanism. *Clim Change* 1997; 35: 1–15.

Hastings WK. Monte Carlo sampling methods using Markov chains and their applications. *Biometrika* 1970; 57: 97–109.

Holt JW, Blankenship DD, Morse DL et al. New boundary conditions for the West Antarctic Ice Sheet: subglacial topography of the Thwaites and Smith glacier catchments. *Geophys Res Lett* 2006; 33: L09502.

Luyendyk BP, Wilson DS, Siddoway CS. Eastern margin of the Ross Sea Rift in western Marie Byrd Land, Antarctica: crustal structure and tectonic development. *Geochem Geophys Geosyst* 2003; 4. https://agupubs.onlinelibrary.wiley.com/doi/10.1029/2002GC000462

MacGregor JA, Fahnestock MA, Catania GA et al. Radiostratigraphy and age structure of the Greenland ice sheet. *J Geophys Res Earth Surf* 2015; 120: 212–41.

Millar D. Acidity levels in ice sheets from radio echo-sounding. *Ann Glaciol* 1982; 3: 199–203.

Morse DL, Blankenship DD, Waddington ED, Neumann TA. A site for deep ice coring in West Antarctica: results from aerogeophysical surveys and thermo-kinematic modeling. *Ann Glaciol* 2002; 35: 36–44.

Rignot E, Mouginot J, Scheuchl B. Ice flow of the Antarctic ice sheet. *Science* 2011; 333: 1427–30.

Robin GDQ, Evans S, Bailey JT. Interpretation of radio echo sounding in polar ice sheets. *Phil Trans R Soc Lond A Math Phys Eng Sci* 1969; 265: 437–505.

Schwander J, Jouzel J, Hammer CU et al. A tentative chronology for the EPICA Dome Concordia ice core. *Geophys Res Lett* 2001; 28: 4243–46.

Siegert MJ, Hodgkinst R, Dowdeswell JA. Internal radio-echo layering at Vostok Station, Antarctica, as an independent stratigraphic control on the ice-core record. *Ann Glaciol* 1998; 27: 360–4.

Young DA, Blankenship DD, Kempf SD et al. Ice thickness and related data over central Marie Byrd Land, West Antarctica (GIMBLE.GR2HI2). *Tech Rep UTIG* 2017. doi:10.15784/601001 https://www.iedadata.org/data/ice-thickness-and-related-data-over-central-marie-byrd-land-west-antarctica-gimble-gr2hi2/

Young DA, Schroeder D, Blankenship D, Kempf SD, Quartini E. The distribution of basal water between Antarctic subglacial lakes from radar sounding. *Phil Trans R Soc A* 2016; 374: 1–21.

Young DA, Wright AP, Roberts JL et al. A dynamic early east Antarctic ice sheet suggested by ice-covered fjord landscapes. *Nature* 2011; 474: 72–5.